




**Effect of initial temperature on compaction and strength of porous silica under shock compression**J. Matthew D. Lane <sup>1,\*</sup>, Jason P. Koski,<sup>1</sup> Keith A. Jones,<sup>1,2</sup> and Tracy J. Vogler <sup>3</sup><sup>1</sup>*Sandia National Laboratories, Albuquerque, New Mexico 87185, USA*<sup>2</sup>*OpenEye Scientific, Santa Fe, New Mexico 87508, USA*<sup>3</sup>*Sandia National Laboratories, Livermore, California 94551, USA* (Received 6 July 2022; revised 14 August 2022; accepted 22 August 2022; published 15 September 2022)

We use molecular dynamics simulation to study the effect of initial temperature on the shock compression of porous silica with densities of 50%, 75%, and full density. We find that the response is strongly influenced by temperature for shocks in a relatively narrow pressure range. Within this range, near the Hugoniot elastic limit, initial preheating from 300 to 1000 K can increase the final shock density by as much as 30%. However, this enhanced densification effect with preheating temperature is negligible at lower pressures (elastic compression), and is equally negligible at higher pressures (strong shock regime). For vitreous silica, the effect of initial temperature is greatest in the compaction regime (pressures between 1 and 3 GPa) where material strength plays a significant role in the mechanical response. Here, preheating can dramatically increase the final density in silica for a given pressure and porosity. Microstructure was found to influence the behavior, with aerogel structures more strongly impacted than nanopowder packings—likely due to the fact that their strengths are more susceptible to thermal softening. For similar reasons, the effect of temperature is greatest in porosities between 50% and 75% density. In some particular cases, the effect of preheating on the Hugoniot can be comparable to increasing porosity by 25%.

DOI: [10.1103/PhysRevB.106.094102](https://doi.org/10.1103/PhysRevB.106.094102)**I. INTRODUCTION**

Silica, or SiO<sub>2</sub>, is one of the most abundant minerals on Earth. Silica exhibits more than 40 crystal structures, such as quartz, tridymite, and cristobalite and is also a ready glass former. Collectively, silicates, in forms ranging from sand and sandstone, to mineral crystals, are estimated to account for at least 60% of the Earth's crust by weight. Thus, silica properties are important to seismology, geology, and planetary science over a wide range of pressures and temperatures. Engineering and commercial applications abound due to silica's properties, ease of processing, and abundance.

Here, our interest is in the high-pressure mechanical response of low-density (i.e., porous, granular, or powder) silica, where applications are common. Much fundamental and applied research has been conducted on sand penetration, and mechanical wave and shock propagation. While interest was intense in the days of underground nuclear testing in desert sands, more recent applications include space and planetary applications, such as in asteroid collision and impact cratering, which can occur in extreme thermal conditions. Temperatures in low Earth orbit range from 100 to 400 K [1], while the mean surface temperature on Venus is 735 K and Mercury can be as hot as 723 K in direct sunlight [2]. These conditions have led to studies of the compressive behavior of both metals [1] and rocks [2] at low and elevated temperatures. Such conditions have been found to affect the cratering behavior under hypervelocity impact. Since many asteroids and comets are not solid bodies it is important to understand

how significant porosity can profoundly influence impact and cratering processes [3,4]. Accurate modeling of cratering processes requires an understanding of material behavior across a wide range of porosities, pressures, and initial temperatures. Recent studies have shown that the temperature of a porous solid affected shock consolidation in SiC and Al<sub>2</sub>O<sub>3</sub> powders, where preheating resulted in better consolidation under explosive loading [5,6].

Silica is an important high-pressure standard in dynamic compression experiments, where quartz [7] and silica aerogel [8] are often used for diagnostic windows, tampers, and pulse-shaping materials. Such uses are common in fundamental science experiments at Sandia National Laboratories where dynamic material response is studied using pulsed-power platforms to achieve remarkably controlled experiments at extreme pressure conditions.

We model conditions found in one-dimensional flyer-plate impact experiments [8–10] of shock traversal through porous media such as in tamped powder beds or aerogel structures. In these experiments, back surface velocimetry is often the primary diagnostic from which wave propagation and material response can be inferred. Drivers can be planar, or corrugated to allow the study of strength.

In a previous study in silica [11] we investigated the enhanced densification of porous silica and explored mechanisms which lead to anomalous behavior under shock compression. We showed that molecular dynamics with the van Beest-Kramer-van Santen (BKS) potential was a reasonable tool to study the qualitative aspects of shocked porous silica.

Our goal in this work is to carefully measure the effect of initial temperature on pore compression dynamics

\*Corresponding author: [jlane@sandia.gov](mailto:jlane@sandia.gov)

TABLE I. Interatomic potential parameters for BKS silica with modified harmonic core.

	$A_{ij}$ (Kcal/mol)	$b_{ij}$ (1/Å)	$c_{ij}$ (Kcal/mol Å <sup>6</sup> )	$F_{ij}^0$ (Kcal/mol/Å)	$V_{ij}^0$ (Kcal/mol)	$K$ (Kcal/mol/Å <sup>2</sup> )	Charge
Si-O	415182.844	4.87318	3079.50877	1187.85	376.5	1000.0	$q_{\text{Si}} = 2.4$
O-O	32026.355	2.76000	4035.6575	1441.37	1372	1000.0	$q_{\text{O}} = -1.2$

under shock loading in porous silica. We use molecular dynamics simulation to model the response of porous SiO<sub>2</sub> under low-pressure shock loading at 0–6 GPa. Molecular dynamics simulation [12,13] is well positioned to address these questions without *a priori* assumptions about the mechanisms. Our shock compression simulations, conducted over a range of porosities and initial temperatures, indicate a complex nonlinear relationship between initial temperature and shock response, which is sensitive not only to density, but also to shock pressure, strength, and microstructure.

In these studies we have been careful to isolate various contributions that preheating can have on shock response. For example, heating an initial sample will cause its density to drop due to thermal expansion of the sample. This change is reversible, i.e., upon cooling the sample returns to its original density. However, as we will discuss, heating can also cause annealing of the porous structure which is not reversible upon cooling. As an example, heating can cause thin cell walls to buckle and collapse, which leads to an irreversible pore collapse. In this case, when the sample is cooled back to its original temperature it will have a higher density. Throughout this study, we have attempted to eliminate irreversible annealing processes. Our primary interest is not in how heating may change the initial material, but rather to understand how changing the initial internal energy alters the processes and mechanisms associated with shock compression of porous silica, and perhaps porous materials, more generally.

## II. METHODOLOGY

We used Sandia’s LAMMPS classical molecular dynamic code [14,15] to model the shock compression dynamics of porous silica. The silica BKS interatomic potential [16] was used, as shown in Eq. (1). The BKS potential is a very well characterized potential which captures much of the behavior of silica glass with a highly efficient two-body interaction, which combines a Coulomb interaction with an exponential core repulsion and a dispersion term. We cut off the exponential and dispersion terms at 1.0 nm and calculated the long-range electrostatics with the particle-particle-particle-mesh algorithm [17] at 10<sup>-4</sup> accuracy. We used a time step of 0.2 fs for all shock and high-temperature simulations, and a time step of 1.0 fs for room-temperature equilibration. The unphysical BKS attractive core was corrected as in Vollmayr *et al.* [18] by replacing the potential with a harmonic core [Eq. (2)] for  $r_{ij} < R_c$ , where  $R_c^{\text{Si-O}} = 1.188$  Å and  $R_c^{\text{O-O}} = 1.441$  Å,

$$V_{ij} = \frac{kq_iq_j}{r_{ij}} + A_{ij}e^{-b_{ij}r_{ij}} - \frac{c_{ij}}{r_{ij}^6}, \quad r_{ij} \geq R_c, \quad (1)$$

$$V_{ij} = \frac{1}{2}Kr_{ij}^2 - F_{ij}^0r_{ij} + V_{ij}^0, \quad r_{ij} < R_c, \quad (2)$$

where  $k$  is a conversion constant and the values for the parameters  $q_i$ ,  $A_{ij}$ ,  $b_{ij}$ ,  $c_{ij}$ ,  $F_{ij}^0$ ,  $V_{ij}^0$ , and  $K$ , given in Table I, are as reported in Refs. [18,19].  $F_{ij}^0$  and  $V_{ij}^0$  were calculated such that the forces and energies are continuous at  $R_c$ . While the BKS potential was not designed for quantitatively accurate high-pressure properties, it has been shown to accurately reproduce silica’s anomalous density temperature dependence [19–21], which is important for modeling the high-temperature states produced in pore collapse. The high-pressure behavior of BKS silica has been shown to reasonably reproduce the solid structure of amorphous silica below 20 GPa [22,23]. However, more advanced potentials [24–27] may better capture various chemical, phase, and liquid properties of silica.

Multiple porous silica systems were built to study a range of porosities and microstructures. Each porous system began from a full-density vitreous silica produced through a melt-quench process from  $\beta$ -cristobalite, as follows. SiO<sub>2</sub> was melted with a linear temperature ramp from 300 to 8000 K over 0.1 ns at constant pressure. The melt was then equilibrated for 2.2 ns at 8000 K and constant volume to remove all residual order from the original crystal, before a linear temperature quench was imposed to 300 K to rapidly resolidify the silica. The final glass density of 2.21 g/cc was a function of the cooling rate, here  $5 \times 10^{11}$  K/s, as described previously [19]. In order to allow very long time (10–50 ns) simulations to be run efficiently, samples were kept to reasonably modest sizes. Two distinct methods for introducing porosity were implemented to mimic two differently structured porous silicas: an aerogel and a sintered nanopowder.

Figures 1(a) and 1(b) show examples of aerogel systems with densities of 50% and 75% of full density, respectively. The aerogel structures were produced by heating the equilibrated full-density glass to the model’s glass transition temperature,  $T_g$ , of approximately 2500 K. At  $T_g$  the glass is solid, but deforms easily rather than responding brittlely. By introducing randomly distributed slow-growing spherical voids, we produced the sinewy aerogel structure. Various final porosities were formed by controlling the void size and number. In LAMMPS, this was accomplished with a “fix indent” command which pushed atoms from the voids with a soft harmonic potential, while the overall system volume expanded with a constant pressure barostat. This process has been described in detail previously [11,28]. Each aerogel contained approximately 372 000 atoms. System dimensions were approximately cubic and periodic with sides between 18 and 30 nm, depending on the aerogel density. A distribution of pore sizes was observed with pore diameters in the range of  $2 \pm 0.5$  nm.

Figures 1(c) and 1(d) show the 4- and 3-nm-diameter sintered nanopowder systems, respectively. The sintered nanopowder structures were produced by aggregation of randomly

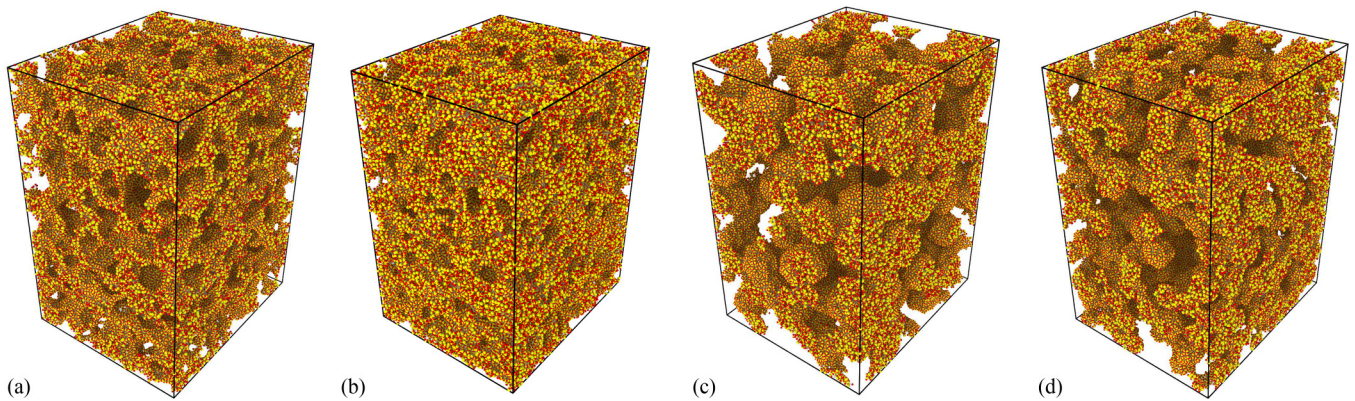


FIG. 1. Four illustrations of atomistic porous silica systems used in these studies. Systems ranged in porosity and microstructure. Snapshots (a) and (b) represent an aerogel structure formed by grown voids to form 50% and 75% density porous systems, respectively. Snapshots (c) and (d) represent a sintered nanopowder structure made from annealing 4- and 3-nm silica glass spheres at 50% overall porosity by density. Silicon and oxygen atoms are colored yellow and red, respectively.

oriented and placed spheres of vitreous silica. Spheres of 3 and 4 nm diameter (i.e., grains) were cut from bulk silica and annealed to relax surface structures. A system was constructed by sequentially placing grains into the periodic simulation box, constraining particles to have some contact with existing grains. Overlapping atoms were removed. While the overall charge neutrality of grains was maintained, local stoichiometry will vary, as at any glass surface. Therefore, local overcoordination and undercoordination is an expected feature of surface contacts between grains. Further, it should be noted that structural stability is not guaranteed in this approach. That is, just as in real powder beds, the material can compact spontaneously when perturbed. Equilibration and annealing of the as-built structure is very important. A simulated “tapping” of the simulations box also helps ensure that the granular contact network is stable. This is accomplished by heating the system to  $T_g = 2500$  K and running in a constant energy ensemble while the box dimensions are varied with a sawtooth volumetric deformation about the desired volume for several nanoseconds. The systems are then cooled to 1000 K at constant volume, and finally allowed to fully relax at constant pressure for several nanoseconds. The final step is to cool the system to the final required temperatures in a constant pressure barostat. This process, unfortunately, does not necessarily deliver a precise predetermined final density, as the stability of the initial packing determines the degree of density relaxation (compaction) before the final stable density is reached. Thus, several systems must generally be constructed and relaxed, and the system with density closest to the desired density is selected for shock studies. Similarly, the range of porosities which can be produced is limited by the stability of the final structures. For this reason, we focus here on nanopowder structures near 50% porosity. The sintered nanopowder systems contain approximately 375 000 atoms and have approximately cubic dimensions with sides between 18 and 25 nm. We believe that the details of this construction technique is not as important as the end result, which is a robust porous structure which is resistant to further spontaneous compaction under thermal cycling.

Our goal is to measure changes to the dynamic response of porous silica due to preheating or precooling. We do not want to convolve the effect of temperature on the initial state. Therefore, as stated earlier, we eliminate the possibility of irreversible structural relaxation processes in the initial state, with a careful thermal cycling check applied to all samples. For each porosity and microstructure we begin with the 1000 K equilibrated system and apply a thermal quench to 300 K in a constant zero pressure ensemble (NPT) over 7 ns (100 K/ns), and hold for 2 ns. We then heat the sample back to 1000 K over 1 ns, then repeat this process for three cycles. If the final 300 K density changes by less than 0.5% over this cycling, then the system is considered stable. Systems that did not pass this test on the first attempt were further annealed at 1000 K until the structure was stable to cycling.

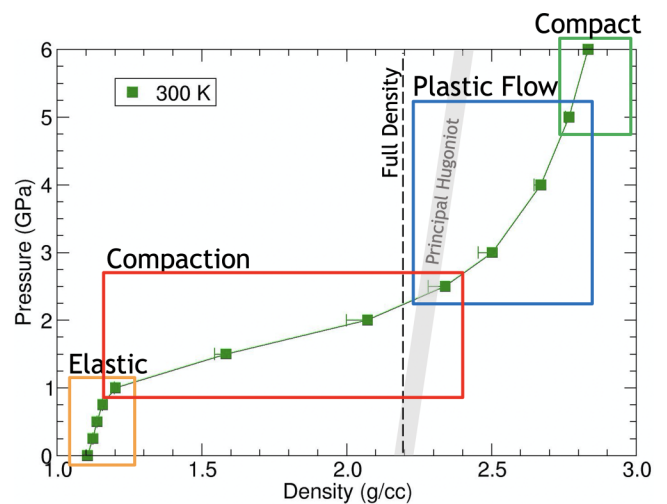


FIG. 2. Hugoniot plot showing applied pressure as a function of final density for 50% porous silica aerogel at an initial temperature of 300 K. The shock response can be characterized by four regimes ranging from elastic, to compaction, to plastic, to fully compact with increasing pressure.



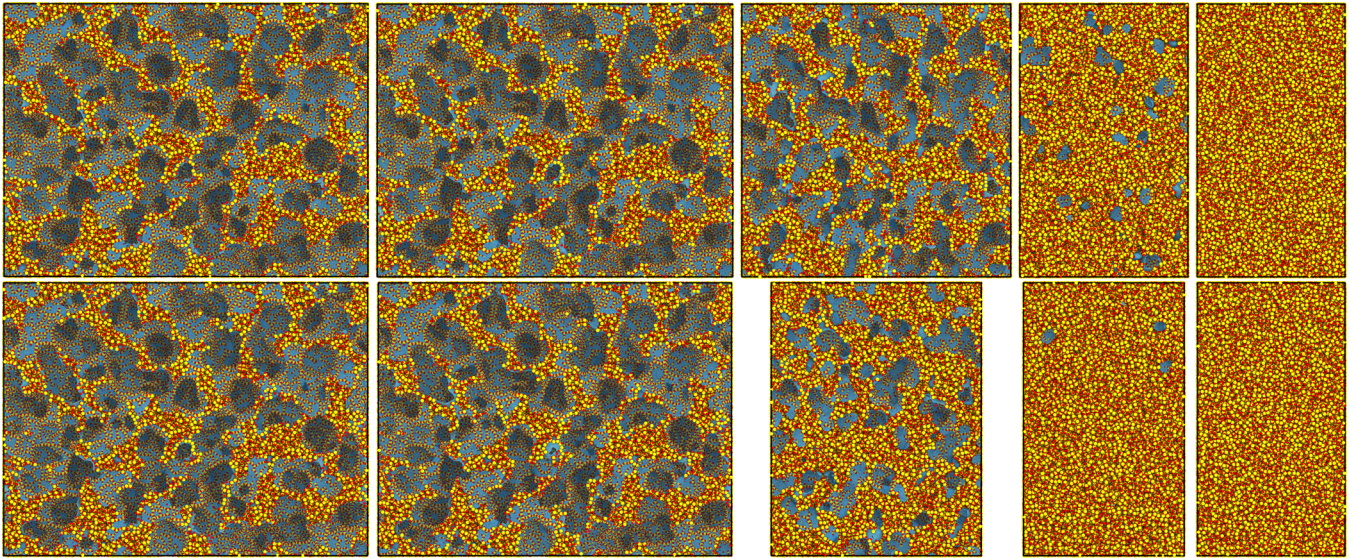


FIG. 3. Final states for 50% porous silica aerogels after compression to final pressures of (from left to right) 0.0, 0.5, 1.5, 3.0, and 5.0 GPa, at two different initial temperatures of (top) 300 K and (bottom) 1000 K. Small voids can be seen to remain up to 5 GPa, above which the material is fully dense. The effect of initial temperature depends on the shock pressure, being largest between 1.0 and 2.0 GPa (compaction regime) and negligible at low- (elastic) and high- (fully dense) pressure regimes.

We found that very slow structural annealing (i.e., upward density creep) is a common trait for all porous systems above 300 K, and must be accounted for. When thermal cycling tests were passed, each system was heated/cooled to four different initial temperatures, 77, 300, 600, and 1000 K.

We use a uniaxial constant-stress Hugoniot method of Ravelo *et al.* [29] to produce shock compressed states. The Hugoniot approach has several distinct advantages. Firstly, because it is a nonpropagating homogeneous method, we are able to efficiently study the system for long times. In addition, the method allows fully periodic representations of the system which is conducive to the handling of long-range electrostatics of the BKS potential. The Hugoniot method has been shown to reproduce, by direct comparison, results of nonequilibrium molecular dynamics (NEMD) methods for similar porous materials [30,31]. Temperature and pressure damping coefficients were  $\beta_H = \beta_p = 20$  ps. Shock compression final states were tested for repeatability by multiple compression runs in orthogonal propagation directions. We found that trial-to-trial variation was less than 2%.

Figure 2 shows a typical Hugoniot for 50% porous silica with four compression regimes annotated. The elastic, compaction, plastic flow, and compact regimes are illustrated in the snapshots in Fig. 3 and more fully described in Sec. III.

The shock front in porous materials is known to be thicker than for fully dense materials. A rule of thumb is that the shock front is at least as thick as the pore length scale, but the shock profiles often include an abrupt rise in pressure and density followed by a more gradual rise to the final state behind the shock front. Especially in the compaction regime, weak shock plasticity can endure for long times ( $> 100$  ns after the shock has passed). While the Hugoniot approach allows us to observe this gradual compaction to much longer times than typical NEMD approaches, we are limited by practicality to 10–50 ns of simulation time. Experimental time

frames are estimated to be up to 500 ns. Figure 4 shows the density vs time plot for several shock simulations. We see a rapid density rise, followed by a slower logarithmic trend (i.e., linear in this linear-logarithmic plot). Density results reported are extrapolated from linear fits out to 500 ns in order to estimate experimentally comparable densities. We follow the same procedure for extrapolating shear stress. This extrapolation is our single largest source of potential error. Error bars in these quantities represent the error which would be introduced if compaction ceased after 100 ns rather than continuing to

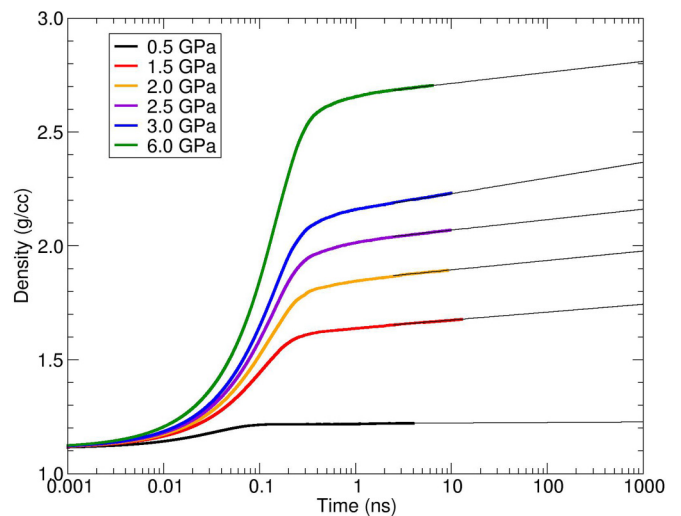


FIG. 4. Hugoniot final density as a function of time for pressures from 0.5 to 6.0 GPa, for a 50% porous silica nanopowder at 300 K. The postshock density rises rapidly, initially, followed by a slower compaction of residual pores. Time profiles exhibit logarithmic compaction trends which are extrapolated to experimentally relevant times of 0.5 ms.



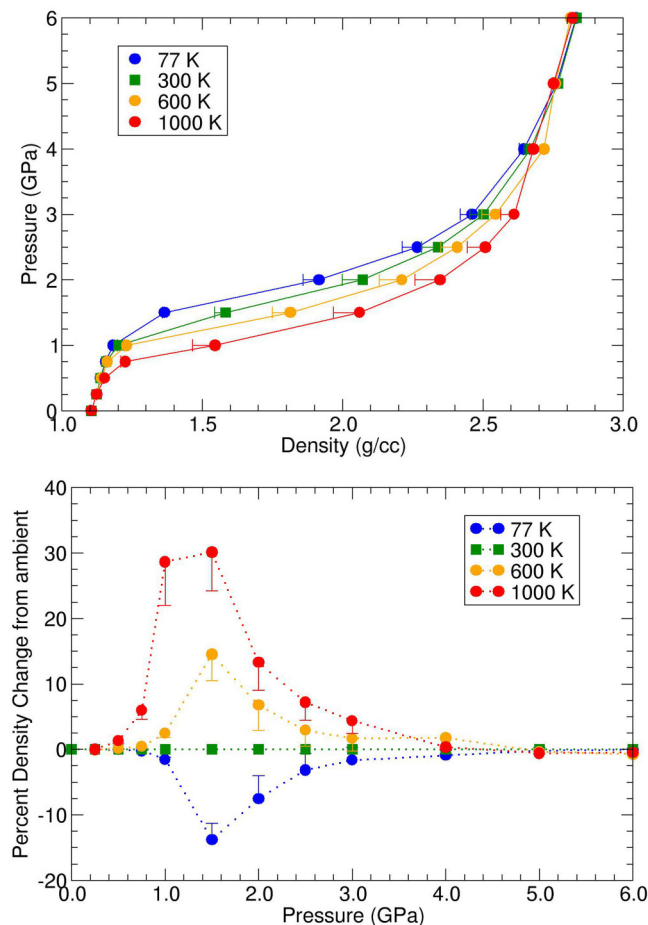


FIG. 5. Top: Hugoniot response in pressure vs density for four initial temperatures ranging from 77 to 1000 K. Bottom: the percent change in the final Hugoniot density compared to the final Hugoniot density for the 300-K reference initial temperature. The maximum effect is a nearly 30% density increase at pressures between 1.0 and 2.0 GPa.

the full 500 ns. Such an early arrest of compaction would lead to lower densities and higher shear stresses. Therefore, plotted densities and shear stresses represent the upper and lower bounds on the expected experimental values of these quantities, respectively.

### III. RESULTS AND DISCUSSION

Figures 2 and 3 show the typical shock response in porous silica aerogel from the perspective of the Hugoniot state variables, and the atomistic structure, respectively. The shock response can be divided into four major regimes. At the lowest pressures is the elastic regime which is characterized by small uniaxial deformation with little to no pore collapse. In this regime the material exhibits strength as shear stresses build with pressure. At higher pressures, beginning just above 1 GPa for the aerogel structure, is the compaction regime in which the voids begin to shrink or collapse; however, the pore collapse is incomplete and continues as a slow process after the shock has passed. Over 3 GPa, the silica aerogel is in the plastic flow regime where many voids are crushed out. In this regime, the Hugoniot density crosses under the

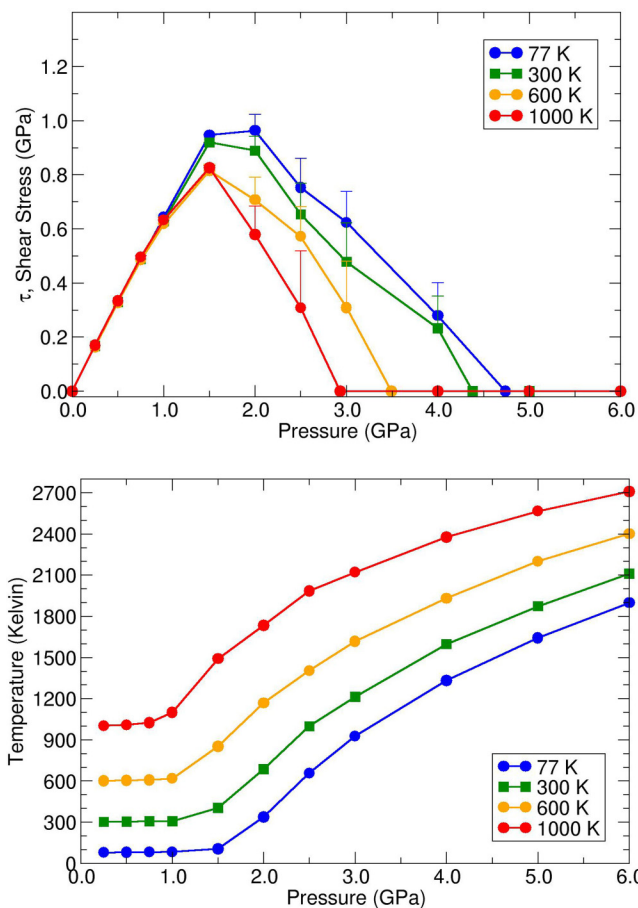


FIG. 6. Top: the final residual shear stress,  $\tau$ , as a function of pressure for various initial temperatures for shock compression of 50% porous aerogel. Bottom: the final temperature as a function of the pressure. The results indicate a loss of strength with increasing initial temperatures beginning at pressures above 1.0 GPa and continuing to melt.

full-density Hugoniot and exhibits enhanced densification. While the overall density of the silica is higher than ambient full density (2.21 g/cc), small voids remain and coexist with highly compressed silica. At the highest pressures is the fully compact regime where, as the name suggests, the voids are fully closed and the material is largely homogeneous. In the fully compact regime, the Hugoniot pressures turn up sharply as the material response stiffens significantly.

Figure 5 (top) shows the effect of initial temperature on the shock Hugoniot for the simulated silica aerogel structure. The four colors indicate the initial equilibrated temperature of the sample before shock loading, which ranged from 77 K (blue) precooled, to 300 K (green) ambient, to 600 K (yellow) and 1000 K (red) preheated. In the compaction regime, at pressures between 1 and 3 GPa, the effect of preheat on the shock compression behavior is dramatic. The peak percent change in density at 1.5 GPa shows that final density increased by 30% for the 1000 K preheated case, as seen in Fig. 5 (bottom). This dramatic change can be attributed to the role of thermal softening in the compaction processes. Within the compaction regime, void walls are beginning to yield and flow, and added tem-

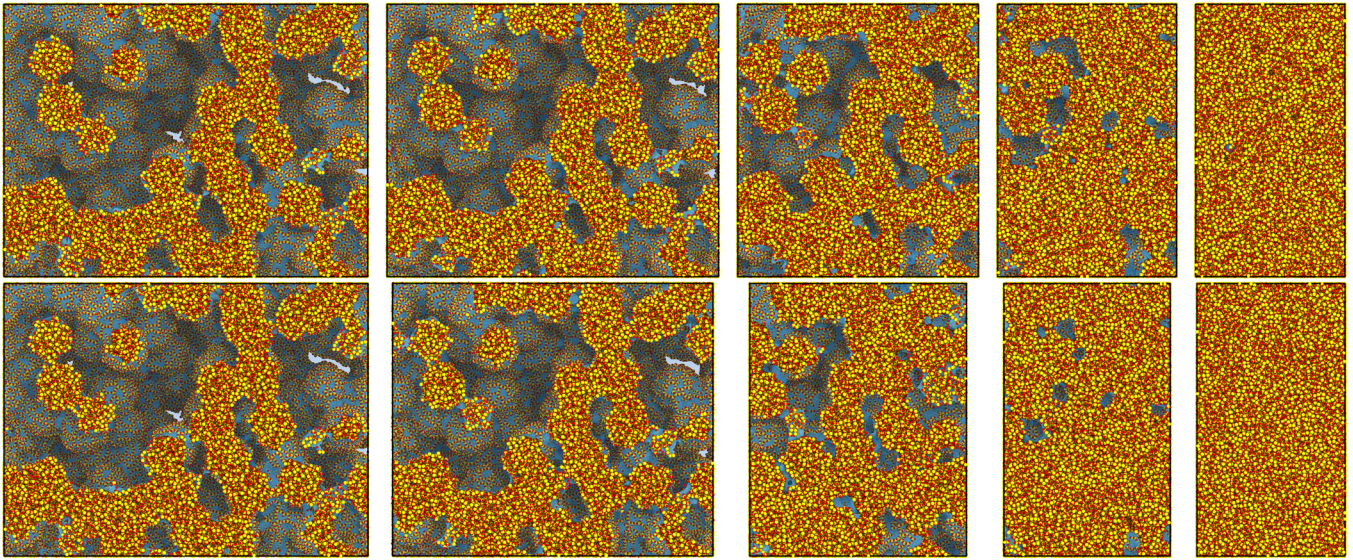


FIG. 7. Final states for 50% porous sintered nanopowder silica after compression to final pressures of (from left to right) 0.0, 0.5, 1.5, 3.0, and 5.0 GPa, at two different initial temperatures of (top) 300 K and (bottom) 1000 K. Small voids can be seen to remain up to 5 GPa, above which the material is fully dense. These systems exhibit immediate plastic deformation (little elastic signature) and the effect of initial temperature, overall, is smaller than for the aerogel structures.

perature shifts the onset of plasticity to lower pressures. Because the Hugoniot slope is shallow in this regime, a small shift in onset pressure leads to significant density increases.

Importantly, the effect of initial temperature is highly dependent on the compression regime. We see, for instance, that at the lowest and highest pressures the Hugoniot is largely unchanged by the initial temperature. In both the elastic and fully compact regimes, the dominant mechanisms are not strongly influenced by initial internal energy, but for different reasons. In the elastic regime, the initial thermal energy is not sufficient to induce plasticity in the pore walls, thus the only thermal effect is thermal expansion which is negligible. In the fully compact regime, the shock is strong and void collapse is complete, or nearly complete, generating significant heating due to hot spot formation. However, the preheat temperature is relatively small in comparison and does not significantly affect the final Hugoniot state.

The effect of strength is illustrated in Fig. 6 where the final residual shear stress of the system  $\tau = \frac{1}{2}[P_z - \frac{1}{2}(P_x + P_y)]$  is plotted versus the uniaxially applied pressure. Again we see that initial temperature has a dramatic effect in reducing the residual shear stress in the system. This reduction of shear stress is due to plasticity and local flow between uniaxial compression and transverse void collapse. The effect can be strong because once pore collapse begins, this process releases additional thermal energy in a positive feedback loop. We see that strength goes to zero in the aerogel system between 3 and 5 GPa, depending on the degree of preheating. This complete loss of residual shear stress is attributed to flow as the material temperature drives upward toward the BKS model's glass transition temperature,  $T_g = 2500$  K.

The bottom plot in Fig. 6 shows that increases in the system temperature are correlated with the drop in residual shear

stress. It is likely that local temperatures in the vicinity of void collapses are much higher than these system averages due to typical hot spot behavior. Shear stress relieving flow is concentrated in these regions.

To assess the role of microstructure, we compared the preheat response of an aerogel structure to a sintered nanopowder packing. We found that the microstructure of the porous material had an effect on the shock compression. Figure 7 illustrates the final states of the 4-nm-diameter grain nanopowder structure for 300 and 1000 K initial temperatures. These snapshots show the same general regimes as for the aerogel, but compared to the aerogel they show less difference between systems with 300 versus 1000 K initial temperatures, even in the compaction regime.

Figure 8 shows two plots of the Hugoniot response. The top image is the pressure as a function of density and the bottom shows the residual shear stress as a function of pressure. The nanopowder Hugoniot plots indicate a noticeably smaller elastic regime, and much less distinct elastic-to-plastic cusp at the Hugoniot elastic limit, compared to the aerogel Hugoniot in Fig. 5. Notably the shear stress indicates that the material shows inelastic response at lower pressures, but is able to retain significant strength to higher pressures than the aerogel. The maximum percent density change due to preheating to 1000 K is only 15% here, compared to 30% in the aerogel.

Figure 9 helps to explain the difference between the elastic-to-plastic transition in the two microstructures. The figure colors the atoms which exhibit significant nonaffine transverse displacement, such as would be created by significant plasticity or other structural relaxation of shear stress. We note that at 1.5 GPa, in the compaction regime, the aerogel shows little plastic displacement at 300 K, and greatly increased plasticity at 1000 K. This behavior can be explained by the preheating leading to significantly enhanced softening of the aerogel, as previously discussed. On the other



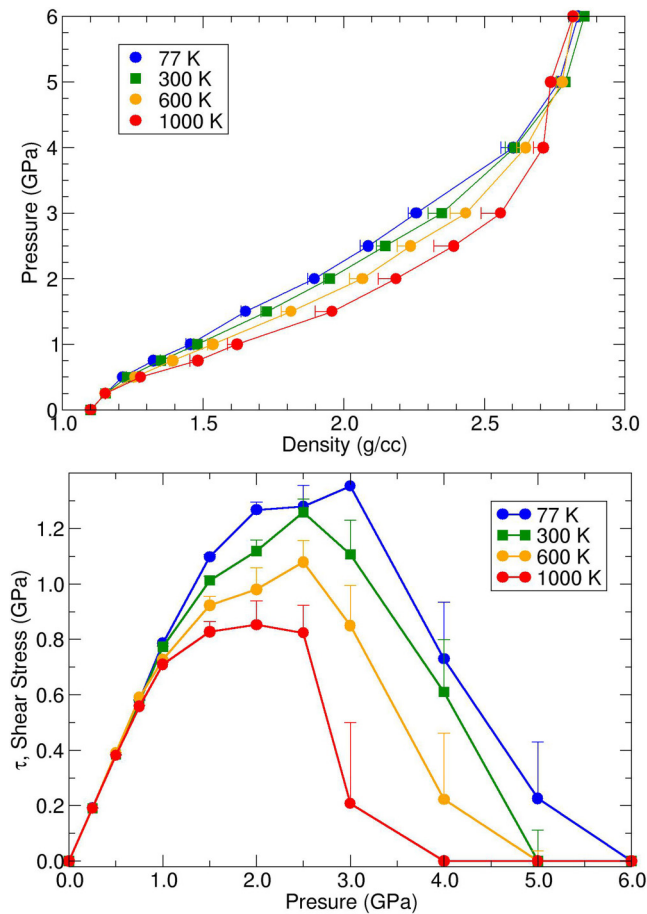


FIG. 8. Hugoniot response for sintered 4-nm nanopowder structures for initial temperatures ranging from 77 to 1000 K (top) in pressure vs density and (bottom) shear stress vs pressure. The nanopowder response shows some significant differences from the aerogel structure.

hand, the nanopowder sample shows significant grain-scale displacement (due to particle rotation, contact slip, etc.) which leads to a much lower plastic onset pressure and indistinct elastic-plastic transition even at 300 K. The figure for 1000 K shows that the plastic response is only slightly enhanced by preheating for the nanopowder.

Finally, by combining varying degrees of porosity with a range of initial temperatures, Fig. 10 shows how aerogel density and preheating can combine to determine shock response. Two important observations can be made. First, that the effect of varying initial temperature appears to be stronger in 75% density systems than in either 50% density or full-density systems. This indicates that there is a peak porosity where preheating plays the most significant role. Second, is that there are combinations of porosity and temperature which give nearly identical shock response. For instance, the Hugoniot response for 75% density material preheated to 1000 K overlaps the Hugoniot response for 50% density material precooled to 77 K.

#### IV. CONCLUSIONS

In conclusion, we have used molecular-scale simulation to explore the mechanisms of pore collapse in shock compressed

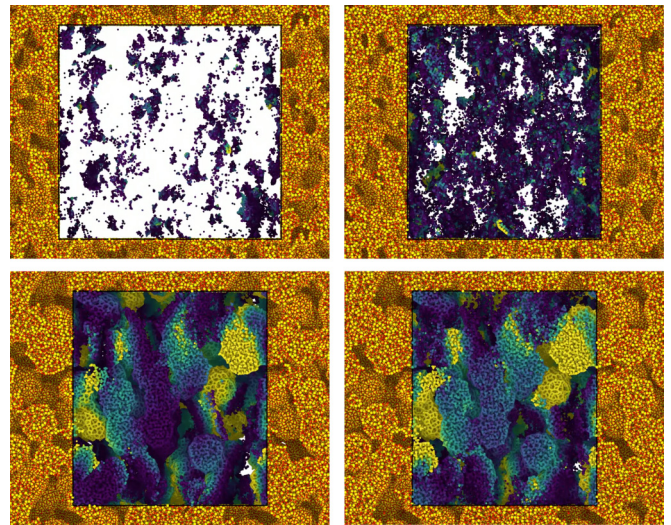


FIG. 9. Snapshots of 1.5 GPa final shock states with atoms in the central window colored to indicate their nonaffine displacement transverse to the shock direction. Nonaffine transverse displacement is an indicator of flow and/or rotation as shear stress relaxation mechanisms (purple for displacements  $\geq 4$  Å to yellow for displacements  $\geq 8$  Å). The top shows aerogel structure and the bottom shows sintered nanopowder structure, both at 50% porosity. Left shows 300 K and right shows 1000 K.

porous silica as a function of initial temperature. We found that temperature can have a dramatic effect on the degree of compaction during shock loading within a relatively narrow range of shock pressures near the Hugoniot elastic limit, while at lower and higher pressures, the effect of initial temperature is negligible. For 50% porous aerogel structures the Hugoniot density can be enhanced by up to 30% for shock pressures between 1 and 3 GPa (i.e., the compaction regime). The effect is found to be correlated to the observed shear stress in the

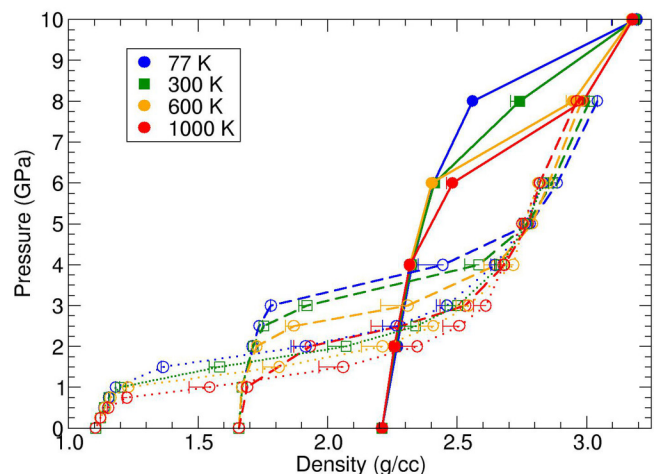


FIG. 10. Hugoniot response in pressure vs density for aerogel structures of three initial porosities, full density, 75%, and 50% density (solid, dashed, and dotted lines, respectively) for initial temperatures ranging from 77 to 1000 K. Initial temperature has as large an effect on the response as initial porosity, in some cases.

material, indicating that temperature leads to softening of the material in this pressure range.

The strong enhancement in compression increases with initial temperature and is strongest at porosities and microstructures in which strength dominates the material response. For instance, we find that aerogels exhibit greater density enhancement than nanopowders. Among aerogels of different densities, the effect is greatest between 50% and 75% of full density.

It is our hope that this work will lead to further study of shock response in materials which are far from room temperature, and that this work will further research in cratering

and hypervelocity debris impact applications in space and planetary science.

#### ACKNOWLEDGMENTS

The authors thank Mark Wilson, at Sandia, for useful discussions. Sandia National Laboratories is a multimission laboratory managed and operated by National Technology & Engineering Solutions of Sandia, LLC, a wholly owned subsidiary of Honeywell International Inc., for the U.S. Department of Energy's National Nuclear Security Administration under Contract No. DE-NA0003525.

- 
- [1] M. Nishida, K. Hayashi, J. Nakagawa, and Y. Ito, *Int. J. Impact Eng.* **42**, 37 (2012).
- [2] A. Morris and M. Burchell, *Procedia Eng.* **204**, 300 (2017).
- [3] K. R. Housen and K. A. Holsapple, *Icarus* **163**, 102 (2003).
- [4] K. R. Housen, W. J. Sweet, and K. A. Holsapple, *Icarus* **300**, 72 (2018).
- [5] S.-S. Shang and M. Meyers, *J. Mater. Sci.* **31**, 252 (1996).
- [6] G. J. Venz, P. Killen, and N. Page, *J. Mater. Sci.* **38**, 2935 (2003).
- [7] M. D. Knudson and M. P. Desjarlais, *Phys. Rev. Lett.* **103**, 225501 (2009).
- [8] M. D. Knudson and R. W. Lemke, *J. Appl. Phys.* **114**, 053510 (2013).
- [9] M. Hudspeth, J. Olles, A. Mandal, J. Williams, S. Root, and T. Vogler, *J. Appl. Phys.* **128**, 205901 (2020).
- [10] C. H. Braithwaite, J. I. Perry, N. E. Taylor, and A. P. Jardine, *Appl. Phys. Lett.* **103**, 154103 (2013).
- [11] K. Jones, J. M. D. Lane, and T. J. Vogler, *AIP Conf. Proc.* **1979**, 050010 (2018).
- [12] B. L. Holian and P. S. Lomdahl, *Science* **280**, 2085 (1998).
- [13] K. Kadau, T. C. Germann, P. S. Lomdahl, and B. L. Holian, *Science* **296**, 1681 (2002).
- [14] A. P. Thompson, H. M. Aktulga, R. Berger, D. S. Bolintineanu, W. M. Brown, P. S. Crozier, P. J. in't Veld, A. Kohlmeyer, S. G. Moore, T. D. Nguyen, R. Shan, M. J. Stevens, J. Tranchida, C. Trott, and S. J. Plimpton, *Comput. Phys. Commun.* **271**, 108171 (2022).
- [15] S. Plimpton, *J. Comput. Phys.* **117**, 1 (1995).
- [16] B. W. H. van Beest, G. J. Kramer, and R. A. van Santen, *Phys. Rev. Lett.* **64**, 1955 (1990).
- [17] R. W. Hockney and J. W. Eastwood, *Computer Simulation Using Particles* (Adam Hilger, 1988).
- [18] K. Vollmayr, W. Kob, and K. Binder, *Phys. Rev. B* **54**, 15808 (1996).
- [19] J. M. D. Lane, *Phys. Rev. E* **92**, 012320 (2015).
- [20] C. A. Angell and H. Kanno, *Science* **193**, 1121 (1976).
- [21] R. Brückner, *J. Non-Cryst. Solids* **5**, 123 (1970).
- [22] J. S. Tse, D. D. Klug, and Y. Le Page, *Phys. Rev. B* **46**, 5933 (1992).
- [23] J. Horbach, *J. Phys.: Condens. Matter* **20**, 244118 (2008).
- [24] A. Takada, P. Richet, C. Catlow, and G. Price, *J. Non-Cryst. Solids* **345-346**, 224 (2004).
- [25] A. Pedone, G. Malavasi, M. C. Menziani, A. N. Cormack, and U. Segre, *J. Phys. Chem. B* **110**, 11780 (2006).
- [26] Y. Yu, B. Wang, M. Wang, G. Sant, and M. Bauchy, *J. Non-Cryst. Solids* **443**, 148 (2016).
- [27] L. C. Erhard, J. Rohrer, K. Albe, and V. L. Deringer, *npj Comput. Mater.* **8**, 90 (2022).
- [28] J. M. D. Lane, *Shock Phenomena in Granular and Porous Materials*, Shock Wave and High Pressure Phenomena, edited by T. Vogler and D. Fredenburg (Springer, Cham, 2019), pp. 231–254, [https://doi.org/10.1007/978-3-030-23002-9\\_8](https://doi.org/10.1007/978-3-030-23002-9_8).
- [29] R. Ravelo, B. L. Holian, T. C. Germann, and P. S. Lomdahl, *Phys. Rev. B* **70**, 014103 (2004).
- [30] J. M. D. Lane, A. P. Thompson, and T. J. Vogler, *Phys. Rev. B* **90**, 134311 (2014).
- [31] J. M. D. Lane, A. P. Thompson, and T. J. Vogler, *AIP Conf. Proc.* **1793**, 120010 (2017).